

Bias voltage dependence of the magnetoresistance in ballistic vacuum tunneling: Theory and application to planar Co(0001) junctions

J. Henk* and P. Bruno

Max-Planck-Institut für Mikrostrukturphysik Weinberg 2, D-06120 Halle (Saale), Germany

(Received 23 May 2003; revised manuscript received 25 August 2003; published 25 November 2003)

Motivated by first-principles results for jellium and by surface-barrier shapes that are typically used in electron spectroscopies, the bias voltage in ballistic vacuum tunneling is treated in a heuristic manner. The presented approach leads in particular to a parametrization of the tunnel-barrier shape, while retaining a first-principles description of the electrodes. The proposed tunnel barriers are applied to Co(0001) planar tunnel junctions. Besides discussing main aspects of the present scheme, we focus in particular on the absence of the zero-bias anomaly in vacuum tunneling.

DOI: 10.1103/PhysRevB.68.174430

PACS number(s): 75.47.Jn, 72.25.Mk, 73.40.Gk

I. INTRODUCTION

At present, extensive efforts are undertaken to employ the electronic spin in “magneto-electronic” devices. This aim challenges especially applied physics, but one is also concerned with model systems of spin-dependent transport in order to understand the basic phenomena.¹ Prototypical devices for studies of ballistic tunneling are planar tunnel junctions (PTJ’s), which consist of two magnetic electrodes separated by an insulating spacer. Of particular interest are the dependencies of the tunnel magnetoresistance (TMR) on the electronic structure of the leads and the spacer, on the width of the spacer, and on the bias voltage.

The conductance of a PTJ depends on the density of states (DOS) of the electrodes and of the tunneling probability of the scattering channels.² The TMR can then be related to the spin polarization of the ferromagnetic electrodes.³ Biasing, which can be viewed as a shift of the chemical potential of one electrode relative to that of the other, enlarges the range of energies in which electrons can tunnel through the spacer and introduces an energy dependence of the electrode spin polarization.

State-of-the-art calculations for spin-dependent tunneling are based on the very successful density-functional theory (DFT).⁴ A bias voltage, however, leads to a nonequilibrium state, which makes it difficult to apply DFT.⁴ An appropriate theoretical description of such a system would require nonequilibrium Green functions (see, e.g., Ref. 5). Therefore a question arises of how one can maintain the *ab initio* framework of electronic-structure calculations, in particular for the leads, but treat the bias voltage in a feasible manner.

Focusing on spin-dependent ballistic tunneling through PTJ’s with finite bias, we investigate in the present work as a simple case tunneling through a vacuum barrier. The electronic properties of the electrodes can still be computed within spin-polarized DFT. The crucial point is the electrostatic potential in the spacer region. Guided by first-principles calculations for jellium⁶ and by theoretical models for surface barriers, we construct tunnel barriers that show the correct asymptotical behavior for large spacer thickness. In particular, one of them compares well with barrier shapes obtained *ab initio* for jellium. The absence of the zero-bias

anomaly (ZBA) in vacuum tunneling of Co(0001) which was recently found by Ding and co-workers^{7,8} lends itself support for an application of the proposed tunnel barrier (for an experimental investigation of Co PTJ’s with an oxide barrier, see Ref. 9). We note in passing that the effect of interface states on vacuum tunneling in fcc-Co(001) was recently investigated theoretically.^{10,11}

The paper is organized as follows. In Sec. II, two heuristic ways of constructing a tunnel barrier (Secs. II B 2 and II B 3) are motivated. Sec. II C deals with computational aspects of calculations for ballistic tunneling. Results for vacuum tunneling between Co(0001) electrodes are discussed in Sec. III.

II. THEORETICAL

A. Surface-barrier shapes of metals

The shape of the surface barrier of a metal was investigated in a vast amount of publications. The possibility to calculate accurately reflected intensities in low-energy-electron diffraction (LEED), which is a particular surface-sensitive spectroscopy, led to several barrier models. Especially at very low energies (VLEED), the shape of the surface barrier has a considerable effect on the LEED $I(V)$ spectra.¹² The free parameters that enter its functional description are fixed by fitting theoretical to experimental data, e.g., to VLEED intensities or to energies of surface and image-potential states.¹³ The latter can be accessed by inverse or by two-photon photoelectron spectroscopy.¹⁴ Note that electronic-structure calculations using the local-density approximation (LDA) do not reproduce the correct image potential in the vacuum.

Regarding electron diffraction, the classical electrostatic potential at a metal surface, with asymptotics $V(z) \approx 1/(4z)$, was investigated by Mac Coll.^{15,16} To avoid the divergence at the metal surface, Cutler and Gibbons¹⁷ proposed a model potential which interpolated between the (constant) inner potential U of the metal and the image-charge potential in the vacuum region. Among the various proposed models, two became the most popular: the so-called JJJ barrier, named after the inventors Jones, Jennings, and Jepsen¹⁸ (see Sec. II B 3 below), and the Rundgren-Malmström (RM) barrier^{19,20} (for a discussion of JJJ and RM

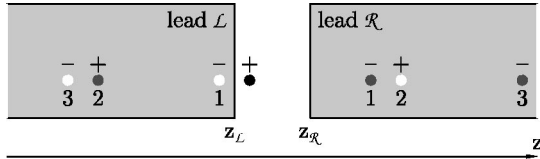


FIG. 1. Method of image charges for two metallic leads (gray areas). The charge $q = +1$ (black circle) is located between the left lead \mathcal{L} (with surface at $z_{\mathcal{L}}$) and the right lead \mathcal{R} (with surface at $z_{\mathcal{R}}$). Two series of image charges are obtained by reflection at the surfaces, starting with reflection either at $z_{\mathcal{L}}$ (white circles) or at $z_{\mathcal{R}}$ (gray circles). Each image charge is indicated by the order of reflection (1,2,3, ...) and the sign of the charge (\pm). Only the first three orders are depicted.

barriers, see Ref. 14). However, electron scattering is a dynamical process and these static shapes hold in principle only for the energy of interest. An energy-dependent generalization of the JJ barrier suggested by Tamura and Feder proved to be successful in describing the image states at the Pd(110) surface.²¹ Further, the atomic structure at the surface leads to a corrugated (three-dimensional) surface potential.^{22–26} However, for most applications the laterally (one-dimensional) and energetically invariant shapes appear to be sufficient.

B. Construction of the tunnel barrier

In this section, we propose two methods of constructing the tunnel barrier. The first method uses the electrostatic potential of a charge between two electrodes (Sec. II B 2), the second approach is a simple superposition of surface potentials (Sec. II B 3).

1. Electrostatic potential between two metal surfaces

Consider a planar tunnel junction with the lead \mathcal{L} occupying the half space $]-\infty, z_{\mathcal{L}}]$, whereas the lead \mathcal{R} fills $[z_{\mathcal{R}}, \infty[$, with $z_{\mathcal{L}} < z_{\mathcal{R}}$ (Fig. 1). The electrostatic potential V_{es} of a charge $q = 1$ (black circle in Fig. 1) between the two semi-infinite metals can easily be obtained by the method of image charges.¹⁶ Because each metal surface acts as a mirror, one has to sum up two infinite series of image-charge potentials (white and gray circles in Fig. 1). This procedure results in

$$V_{\text{es}}(z) = \frac{1}{4(z_{\mathcal{R}} - z_{\mathcal{L}})} \left[2\gamma + \Psi\left(\frac{z - z_{\mathcal{L}}}{z_{\mathcal{R}} - z_{\mathcal{L}}}\right) + \Psi\left(\frac{z_{\mathcal{R}} - z}{z_{\mathcal{R}} - z_{\mathcal{L}}}\right) \right],$$

$$z \in]z_{\mathcal{L}}, z_{\mathcal{R}}[. \quad (1)$$

Here, $\gamma \approx 0.577216$ is Euler's constant and Ψ denotes the digamma function.²⁷ The latter is the logarithmic derivative of the gamma function $\Gamma(z)$, $\Psi(z) = d\ln\Gamma(z)/dz$, with $\Psi(1) = -\gamma$, $\Psi(z) \propto \ln z$ for $z \rightarrow \infty$, and $\Psi(z) \propto -\gamma - 1/z$ for $z \rightarrow 0^+$. Obviously, V_{es} diverges for $z \rightarrow z_{\mathcal{L}}$ and $z \rightarrow z_{\mathcal{R}}$. It shows further the well-known asymptotics for the presence of a single metallic lead. For example, expanding V_{es} in a power series around $z = z_{\mathcal{R}}$ yields

$$\lim_{z_{\mathcal{L}} \rightarrow -\infty} V_{\text{es}}(z) = -\frac{1}{4(z_{\mathcal{R}} - z)}, \quad z \in]-\infty, z_{\mathcal{R}}[. \quad (2)$$

Considering only the first-order approximation for V_{es} , i.e., the direct images of the charge q (labeled 1 in Fig. 1),

$$V_{\text{es}}^{(1)}(z) = -\frac{1}{4} \left[\frac{1}{z - z_{\mathcal{L}}} + \frac{1}{z_{\mathcal{R}} - z} \right], \quad z \in]z_{\mathcal{L}}, z_{\mathcal{R}}[, \quad (3)$$

one sees that V_{es} represents a higher barrier than $V_{\text{es}}^{(1)}$ because the images of even order produce an additional repulsion (“+” in Fig. 1).

2. Image-charge potential as tunnel barrier

The electrostatic potential between two semi-infinite jellium metals including a bias voltage was calculated self-consistently within DFT by Lang.⁶ He found that even with finite bias the potential in the electrodes is constant a few Bohr radii (a_0) apart from the respective surfaces. Further, the divergence of the classical image-charge potential V_{es} at $z_{\mathcal{L}}$ and $z_{\mathcal{R}}$ is bridged over by a smooth interpolating function which shows the form of a typical LEED-motivated surface barrier (cf. Sec. II A). And last, application of a bias voltage apparently produces a linear potential drop in the spacer region [cf. Fig. 2(b) in Ref. 6]. Guided by these findings we construct in the following a tunnel barrier by means of the classical electrostatic potential [Eq. (1)] and by LEED-type surface potentials.

To avoid the divergences of the electrostatic potential V_{es} , a smooth continuous interpolating function between the image-charge potential and the inner potentials of the leads, $U_{\mathcal{L}}$ and $U_{\mathcal{R}}$, is used (the vacuum energy is taken as energy zero). For this paper we choose a Lorentzian shape²⁵ but any other reasonable shape can be used, too (see Sec. II A). The interface potential V_{if} then reads

$$V_{\text{if}}(z) = \begin{cases} -U_{\mathcal{L}} & z \in]-\infty, z_{\mathcal{L}}^c] \\ \alpha_{\mathcal{L}} [1 + \beta_{\mathcal{L}}(z - z_{\mathcal{L}}^c)^2]^{-1} + \gamma_{\mathcal{L}} & z \in [z_{\mathcal{L}}^c, z_{\mathcal{L}}^v] \\ V(z) & z \in [z_{\mathcal{L}}^v, z_{\mathcal{R}}^v] \\ \alpha_{\mathcal{R}} [1 + \beta_{\mathcal{R}}(z - z_{\mathcal{R}}^c)^2]^{-1} + \gamma_{\mathcal{R}} & z \in [z_{\mathcal{R}}^v, z_{\mathcal{R}}^c] \\ -U_{\mathcal{R}} & z \in [z_{\mathcal{R}}^c, \infty[\end{cases}. \quad (4)$$

The coordinates $z_{\mathcal{L}}^c$, $z_{\mathcal{L}}^{\text{im}}$, and $z_{\mathcal{L}}^v$ specify the positions of the onset of the interpolating Lorentzian, of the divergence of the potential V , and of the transition to V with respect to \mathcal{L} (Fig. 2). They have to be obtained by comparing theoretical results with other data, e.g., surface-state energies, VLEED spectra, etc., for the surface system (i.e., in the limit $z_{\mathcal{R}} \rightarrow \infty$). The parameters $\alpha_{\mathcal{L}}$, $\beta_{\mathcal{L}}$, and $\gamma_{\mathcal{L}}$ are fixed by the conditions of smooth continuity in $z_{\mathcal{L}}^c$ and $z_{\mathcal{L}}^v$. Analogous considerations apply for the lead \mathcal{R} . The potential V in the interior of the spacer can be chosen to incorporate the electrostatic potential between two metal electrodes, V_{es} , and the bias voltage as well, as being discussed in the following.

Bringing two metals so close that electrons can tunnel from one metal to the other aligns the Fermi levels of the two

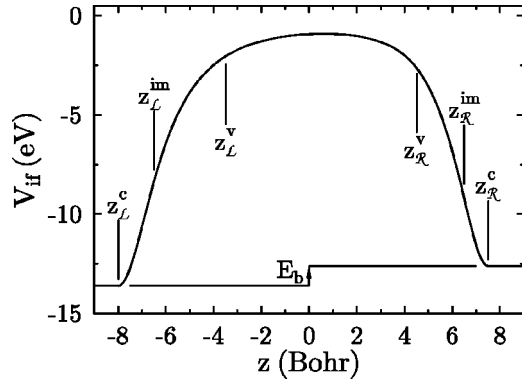


FIG. 2. Image-charge potential as tunnel barrier. The barrier shape is defined by the parameters as indicated [cf. Eq. (4)]. The Lorentzian shapes extend over the ranges $[z_L^c, z_L^v]$ and $[z_R^v, z_R^c]$ and connect smoothly to the electrostatic potential in $[z_L^v, z_R^v]$. The latter comprises the image-charge potential V_{es} [Eq. (1)] as well as the bias potential V_b [Eq. (6)]. The inner potentials $U_L = 13.61$ eV and $U_R = 12.61$ eV for the left and the right lead, respectively, determine the bias voltage E_b to +1 eV.

leads. This energy shift is given by the contact potential $\Phi_L - \Phi_R$, i.e., the difference of the work functions Φ_L of \mathcal{L} and Φ_R of \mathcal{R} . Note that the alignment of the Fermi levels is accompanied by a shift of the inner potentials, that is, e.g., U_R of the semi-infinite system is replaced by $U_R - \Phi_L + \Phi_R$. Since $V(z)$ was not specified explicitly in Eq. (4), it can account for the contact potential and the bias voltage,

$$V(z) = V_{es}(z) + V_b(z). \quad (5)$$

Here, V_{es} is the electrostatic potential from Eq. (1) and V_b is the bias, for which a linear drop over the interface region is assumed:

$$V_b(z) = \begin{cases} 0 & z \in]-\infty, z_L^c[\\ E_b \frac{z - z_L^c}{z_R^c - z_L^c} & z \in [z_L^c, z_R^c] \\ E_b & z \in [z_R^c, \infty[\end{cases} \quad (6)$$

This ansatz is motivated by the fact that the electric field is well screened within the electrodes but unscreened within the vacuum spacer.

Figure 3 presents a series of tunnel barriers in dependence of the lead separation $z_R^c - z_L^c$. The heights of the barriers increase with separation (for an experimental estimation of the barrier height vs distance, see Ref. 7). As already mentioned, taking the first-order approximation $V_{es}^{(1)}$ instead of V_{es} leads to a reduced height (cf. the dashed line for 15 a_0 lead separation). The shape dependence on the bias is addressed in Fig. 4. For rather large bias, the linear potential drop in the interface region can be clearly retrieved. We note in passing that the present construction produces potential shapes that compare qualitatively well with those obtained *ab initio* for jellium by Lang.⁶ Further, a similar approach was recently used to explain the Stark shifts of surface states in scanning tunneling spectroscopy.²⁸

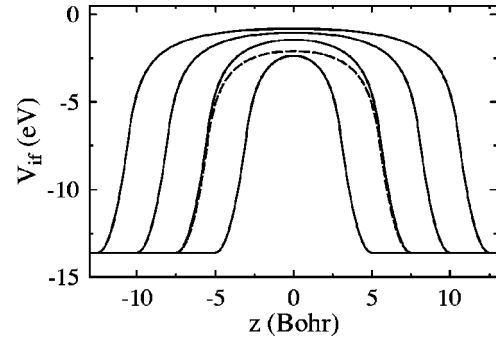


FIG. 3. Dependence of the interface potential V_{if} [Eq. (4)] on the lead separation. The barriers with electrostatic potential V_{es} [Eq. (1)] are shown for separations of 10, 15, 20, and 25 a_0 (Bohr radii) at zero bias (solid; $E_b = 0$ eV). In addition, a barrier with first-order approximation potential $V_{es}^{(1)}$ [Eq. (3)] is shown for 15 a_0 separation (dashed). The inner potentials of the leads are equal ($U_L = U_R = 13.61$ eV).

One advantage of the present approach is that the height of the tunnel barrier is automatically adjusted in dependence on the lead separation and on the bias voltage. Further, the barrier shape shows the correct image potential asymptotics for large lead separation [cf. Eq. (3)]. In turn, the approach should not be applied for too small separations because the barrier shape would significantly differ from the interface potential which would be obtained from a self-consistent calculation for a narrow tunnel junction. This, however, could possibly be compensated by adjusting the parameters z_L^c, \dots, z_R^c not for the semi-infinite system but for the narrow junction.

3. Superposition of surface barriers

For large lead separations and small bias voltages, the probability of electrons to tunnel from one lead to the other

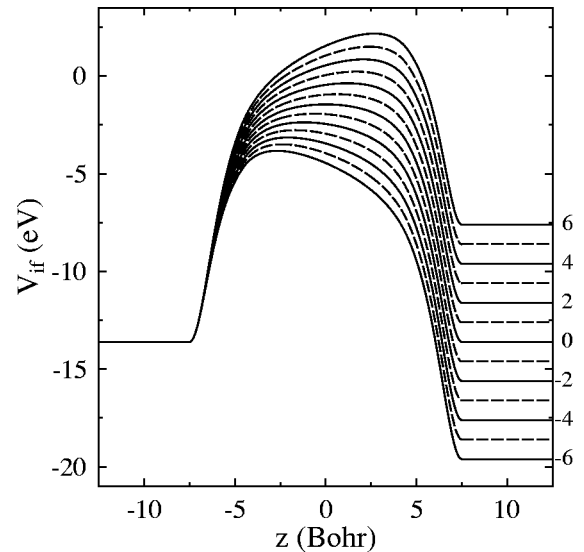


FIG. 4. Dependence of the interface potential V_{if} [Eq. (4)] on the bias. For a lead separation of 15 a_0 (Bohr radii), the right lead \mathcal{R} is biased from -6 eV to +6 eV (as indicated on the right; alternating solid and dashed lines; $U_L = U_R = 13.61$ eV).

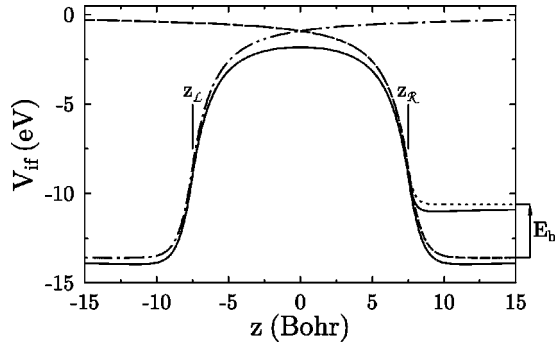


FIG. 5. Formation of an interface barrier by superposition of surface barriers. Without bias, two surface barriers of JJJ type (\mathcal{L} dashed-dotted and \mathcal{R} dashed) are superposed to yield the interface barrier (solid). The inner potentials are equal ($U_{\mathcal{L}}=U_{\mathcal{R}}=13.61$ eV). The application of a bias shifts the inner potential of \mathcal{R} (dotted; $E_b=3$ eV, cf. the arrow) and results in the other tunnel barrier (also solid). The positions of the image-potential divergences are $z_{\mathcal{L}}=-7.5 a_0$ and $z_{\mathcal{R}}=7.5 a_0$ (Bohr radii), respectively, $\lambda_{\mathcal{L}}=\lambda_{\mathcal{R}}=1.25/a_0$ [Eq. (8)]. The vacuum level is taken as energy zero.

is very small. Hence, in a self-consistent calculation for a tunnel junction, the tunnel barrier appears to be almost exclusively determined by the electron density of the respective lead and not significantly influenced by that of the other lead. This consideration might lead one to construct a tunnel barrier by superposition of the respective surface barriers,

$$V_{\text{if}}(z) = V_{\mathcal{L}}(z) + V_{\mathcal{R}}(z), \quad (7)$$

where $V_{\mathcal{L}}$ and $V_{\mathcal{R}}$ are the surface potentials of the respective leads. Taking JJJ barriers,¹⁸ one arrives at

$$V_{\mathcal{L}}(z) = \begin{cases} \frac{1}{4(z_{\mathcal{L}}-z)} [1 - \exp[\lambda_{\mathcal{L}}(z_{\mathcal{L}}-z)]] & z \in [z_{\mathcal{L}}, \infty[\\ -\frac{U_{\mathcal{L}}}{\alpha_{\mathcal{L}} \exp[\beta_{\mathcal{L}}(z_{\mathcal{L}}-z)] + 1} & z \in]-\infty, z_{\mathcal{L}}] \end{cases} \quad (8)$$

for the surface barrier of \mathcal{L} . The values of $\alpha_{\mathcal{L}}$ and $\beta_{\mathcal{L}}$ are determined by requiring smooth continuity at $z=z_{\mathcal{L}}$. Because $U_{\mathcal{L}}$ is known from the self-consistent calculation for the surface system, $z_{\mathcal{L}}$ and $\lambda_{\mathcal{L}}$ remain as the only parameters to be adjusted. For the surface potential of \mathcal{R} one obtains an analogous form.

The simple superposition of surface barriers appears to be problematic for heterojunctions or biased junctions. In both cases, the relative energy shift of one electrode, say \mathcal{R} , results in a finite potential which extends into the entire other electrode \mathcal{L} . This is due to the fact that the surface potential of \mathcal{R} extends infinitely far into \mathcal{L} . One way to overcome this problem is to take the bias only as an energy shift in the interior of \mathcal{R} , that is, to replace the inner potential $U_{\mathcal{R}}$ by $U_{\mathcal{R}} - E_b$. Figure 5 shows such a superposition of JJJ surface barriers. The inner potential of \mathcal{R} is shifted by $E_b=3$ eV (cf. the arrow). Apparently, the barrier shape does not change

significantly with bias in $[z_{\mathcal{L}}, z_{\mathcal{R}}]$, in contrast to the former construction (Fig. 4). In particular, the linear potential drop is not observed.

4. Résumé

The two construction recipes result in tunnel barriers with different features. While the more elaborate one [Eq. (4)] produces barrier shapes which are qualitatively close to those obtained from first-principles for jellium,⁶ the barriers of the superposition approach [Eq. (7)] lack most of these important features. In particular, the linear potential drop in the spacer region is missing. Both approaches can easily be extended to energy-dependent and corrugated (three-dimensional) tunnel barriers.

Wang and co-workers obtained the shape of the tunnel barrier by matching two surface systems that were calculated for equal but opposite shifts of the work functions.¹¹ The resulting bias-dependent barriers agree well with that shown in Fig. 4.

C. Computational aspects of ballistic tunneling

For the ballistic-tunneling calculations we applied the layer-KKR (Korringa-Kohn-Rostoker) approach of MacLaren and co-workers²⁹ which is based on the Landauer-Büttiker result for the tunnel conductance.³⁰ At a given energy E and in-plane crystal momentum \vec{k}_{\parallel} , one computes the Bloch states $n_{\mathcal{L}}$ and $m_{\mathcal{R}}$ of the electrodes \mathcal{L} and \mathcal{R} and classifies them with respect to their propagation direction: to the right (+) or to the left (-). The scattering matrix S of the spacer \mathcal{S} is first computed in a plane-wave basis using LEED algorithms (like layer doubling and layer stacking; see, for example, Ref. 31) and subsequently expressed in terms of the scattering channels, i.e., in the Bloch-state basis. The transmission $T(E_t, \vec{k}_{\parallel})$ at the tunnel energy E_t is then a sum over all pairs of Bloch states that are incident in \mathcal{L} and outgoing in \mathcal{R} ,

$$T(E_t, \vec{k}_{\parallel}) = \sum_{n_{\mathcal{L}}, m_{\mathcal{R}}} |S_{n_{\mathcal{L}} m_{\mathcal{R}}}^{++}(E_t, \vec{k}_{\parallel})|^2. \quad (9)$$

The above sums comprise both majority- and minority-spin Bloch states and thus $T(E_t, \vec{k}_{\parallel})$ contains the spin summation implicitly. The tunnel conductance $G(E_t)$ is obtained by summing over the two-dimensional Brillouin zone (2BZ),

$$G(E_t) = G_0 \sum_{\vec{k}_{\parallel} \in 2\text{BZ}} T(E_t, \vec{k}_{\parallel}). \quad (10)$$

Here, $G_0 = e^2/h$ is the quantum of conductance which equals $1/(2\pi)$ in atomic units.¹⁶ Adaptive mesh refinement provides an efficient method to obtain accurate and well-converged 2BZ sums, in particular, if small parts of the 2BZ contribute significantly to the conductance.³²

With a bias voltage applied, electrons can tunnel from occupied states of one lead into unoccupied states of the other lead. The total conductance is then obtained by integrating over the energy interval given by the Fermi energies E_F of the electrodes. The averaged conductance thus reads

$$G_{\text{av}} = \frac{1}{|E_{\text{FL}} - E_{\text{FR}}|} \int_{\min(E_{\text{FL}}, E_{\text{FR}})}^{\max(E_{\text{FL}}, E_{\text{FR}})} G(E_t) dE_t. \quad (11)$$

The tunnel magnetoresistance (TMR) ρ is defined as the asymmetry of the (averaged) conductances for parallel (P) and antiparallel (AP) alignment of the electrode magnetizations,

$$\rho = \frac{G_{\text{av}}(\text{P}) - G_{\text{av}}(\text{AP})}{G_{\text{av}}(\text{P}) + G_{\text{av}}(\text{AP})}. \quad (12)$$

To treat in practice the bias voltage we proceed as follows. First, self-consistent electronic-structure calculations for the semi-infinite leads \mathcal{L} and \mathcal{R} generated muffin-tin (MT) potentials of the bulk, of the surface, and in the vacuum region. The MT zeroes were taken as inner potentials $U_{\mathcal{L}}$ and $U_{\mathcal{R}}$, respectively (the MT zero is the constant potential in the interstitial region). For each of the leads, the MT potentials in the vacuum region were replaced by a smooth surface barrier, the parameters of which were obtained as follows.

The spectral densities (SD's) of the surface layers obtained from an *ab initio* calculation served as reference to which the SD's obtained for the corresponding system but with a smooth surface barrier were compared. The parameters of the smooth barrier were modified until the SD's were in agreement. The focus laid in particular on the energy range used in the subsequent tunneling calculations and on surface states. For Co(0001), an important feature is the energy of the majority surface state at $\vec{k}_{\parallel}=0$ [cf. Fig. 2(b) in Ref. 8; see also Refs. 33–35]. It turned out that the latter is very sensitive to the shape of the smooth surface barrier (according to the so-called “round-trip criterion” of the phase-accumulation model for surface states or quantum-well states,³⁶ it depends on the reflectivity of the surface barrier).

Having fixed the barrier parameters, the tunnel junction was built from the bulk and surface potentials of the two electrodes and the interface barrier [Eqs. (4)–(6)]. Besides the smooth interface barrier, the spacer \mathcal{S} comprises all layers with MT potentials that differ from the respective bulk potentials. In example, for a Co(0001) tunnel junction the first four layers on either side of the smooth tunnel barrier were used. The bias was taken into account by shifting the inner potential of one of the leads (muffin-tin zero) and determining the barrier shape [Eq. (1)]. The smooth barrier V_{if} was treated as a single layer in the multiple-scattering calculations. Its scattering matrix S was obtained within the propagator formalism.³⁷

The surface barrier of the semi-infinite leads is represented by MT potentials in the *ab initio* calculations. Therefore it contains a corrugation, i. e., an in-plane asymmetry of the barrier potential. The smooth barriers used in the present work did, however, not account for a corrugation. Since the main effect on the SD's is due to the barrier shape along the surface normal, the influence of the corrugation is regarded as of minor importance, in particular at closed-packed metal surfaces.

As usual for the KKR method, a small imaginary part η has to be added to the energy E ,³⁸ leading in general to

complex wave numbers k_{\perp} .^{39,40} Therefore the electrode eigenfunctions are no longer true Bloch states but become evanescent states [$\text{Im}(k_{\perp}) \neq 0$]. Eigenstates stemming from Bloch states [$\text{Im}(k_{\perp}) = 0$ for $\eta = 0$] show typically the smallest $\text{Im}(k_{\perp})$ and can therefore be separated from evanescent states [$\text{Im}(k_{\perp}) \neq 0$ for $\eta = 0$].²⁹ In the spacer \mathcal{S} , the nonzero η leads to damping in addition to the intrinsic one, artificially enhancing the decay of the conductance with spacer thickness. Further, the scattering matrix S is no longer unitary and hence the total current is not conserved. Therefore one has to choose η carefully in order to produce reliable results. We found that a value of $\eta = 10^{-4}$ eV produces no considerable artefacts.

The Landauer-Büttiker approach used here avoids the computation of the Green function of the complete system, which is in particular problematic for a nonequilibrium system. Considering the asymptotic transmission channels (Bloch states), states that are localized at the barrier do not contribute to the transmission.

Recently, Davis and MacLaren reported on model calculations for spin-dependent tunneling at finite bias.⁴¹ In their work, however, the electronic structure of the Fe electrodes was approximated by plane waves, whereas the barrier was assumed as steplike with a linear drop. Although conceptual similar, our approach goes beyond that work. First, the electrodes are treated on a first-principles level. Second, the barrier shows the correct asymptotics (for the free surfaces) and, once the shape parameters are fixed, depends automatically on both lead separation and bias.

III. RESULTS FOR Co(0001)

Recently, Ding and co-workers investigated the bias-voltage dependence of the TMR with a spin-polarized scanning tunneling microscope (STM).⁸ In contrast to tunneling through oxide barriers, they observed no zero-bias anomaly (ZBA), i. e., a (rather) sharp maximum of the TMR at zero bias (see, for example, Ref. 42). With a vacuum barrier replacing an oxide barrier, the TMR appeared to be almost constant. This finding suggests that the ZBA is mainly due to imperfections in oxide barriers, rather than to scattering at magnons and spin excitations (in the leads). Further, the so-called DOS effect, i. e., the energy dependence of the spin-resolved density of states of the leads, proved to be small in the case of Co(0001).

The experimental findings of Ding *et al.* were corroborated by ballistic tunneling calculations for planar Co(0001) junctions as sketched in Sec. II C. The tunnel barrier was taken as a superposition of surface barriers (Sec. II B 3). In the present work, we focus on corresponding calculations but for the more elaborate image-charge potential (Sec. II B 2).

The calculations of Ref. 8 and of the present work differ mainly in the used interface barriers: the superposition of JJJ barriers (Ref. 8) and the more sophisticated image-potential approach (Sec. II B 2). The potentials of the Co electrodes were identical. Although the parameters of the tunneling calculations differed slightly [e. g., the number of \vec{k}_{\parallel} used in the 2BZ integration, Eq. (10)], the results of both calculations are comparable and of the same accuracy. Since both calcu-

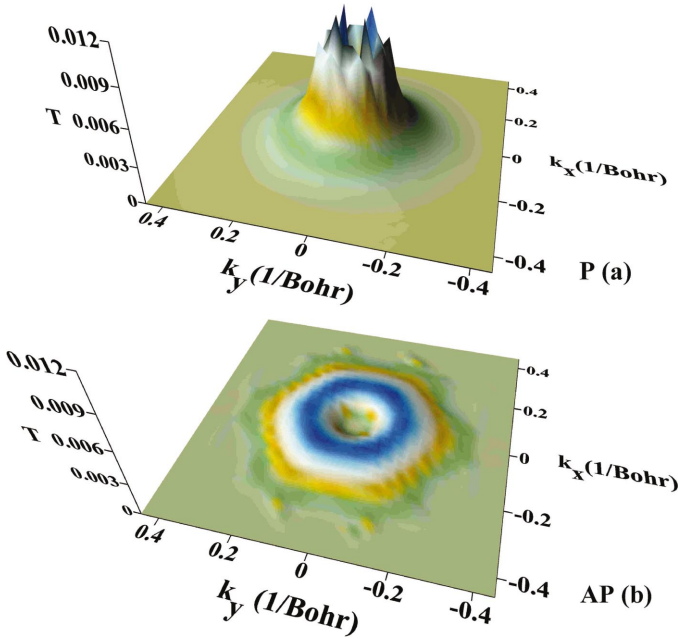


FIG. 6. (Color) Transmission $T(E_F, \vec{k}_{\parallel})$ of vacuum tunneling in Co(0001) for P [(a), top] and AP [(b), bottom] alignment of the lead magnetizations. For 0-eV bias, the lead separation was chosen as 7.52 Å. The maximum transmission is about 0.01 (P alignment). Both panels share the same scale. Note that only the central part of the two-dimensional Brillouin zone is displayed.

lations rely on the same electrode potentials, the band structure and the spectral density shown in Ref. 8 can be consulted for the interpretation of the results presented in the following.

The transmission $T(E_t, \vec{k}_{\parallel})$, Eq. (9), depends on the relative orientation of the lead magnetizations (P and AP), as is shown for 0 eV bias (tunneling at E_F) in Fig. 6. For the chosen lead separation of 7.52 Å, only those Bloch states with a \vec{k}_{\parallel} in the central part of the 2BZ contribute significantly to the transmission. The normal component of the wave vector within the tunnel barrier, $k_{\perp}(z) = \sqrt{2[E_F - V_{it}(z)] - \vec{k}_{\parallel}^2}$, is imaginary and gives rise to strongly evanescent states in the tunnel barrier for Bloch states with large \vec{k}_{\parallel} , and thus to a small transmission. For Bloch states with \vec{k}_{\parallel} near $\bar{\Gamma}$ (i.e., $\vec{k}_{\parallel} = 0$), the decay within the barrier is less and the transmission can be larger. In total, this results in a “focusing” of $T(E_t, \vec{k}_{\parallel})$ at the 2BZ center.

Both the P and the AP case show minor transmission close to $\bar{\Gamma}$. These minima are surrounded by ringlike structures of increased transmission. The maximum P transmission is larger than for AP alignment (by a factor of about 10), but the AP transmission displays a broader ring compared to the P transmission.

When integrated over the 2BZ, one finds that $G(P) > G(AP)$ (Fig. 7 for zero bias). With increasing bias, the conductances for tunneling at $E_t = E_{FL}$ decrease. Since ballistic tunneling is a phase coherent process, shifting of the electronic states of one electrode relative to those of the other by the bias might reduce the phase coherence, or the spin-

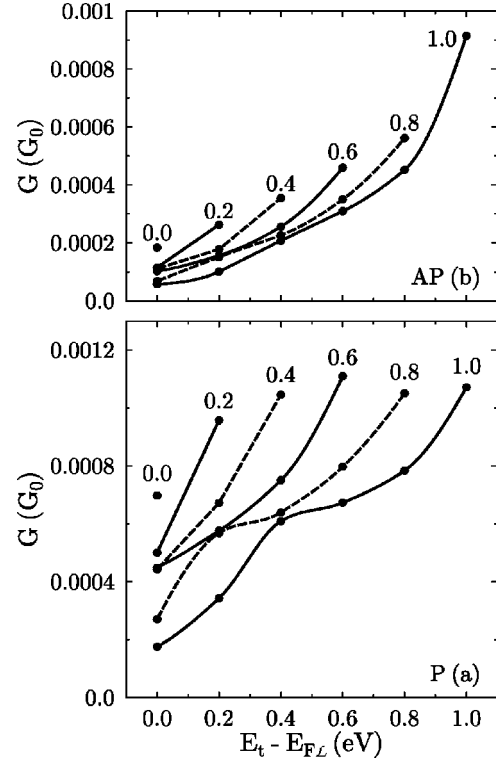


FIG. 7. Ballistic conductance G (in units of G_0 , the quantum of conductance) vs tunnel energy E_t in Co(0001) for P [(a), bottom] and AP [(b), top] alignment. The bias E_b ranges from 0.0 to 1.0 eV and is indicated at the top of each data set. E_{FL} is the Fermi energy of lead \mathcal{L} .

dependent DOS in the relevant region of the 2BZ decreases with energy. We checked the spectral density carefully but found no significant feature that would corroborate unequivocally the latter explanation.

The transmissions $T(E_t, k_{\parallel})$ show ringlike structures (Fig. 6), the radii of which increase with tunnel energy. The ring area, i.e., the area in the 2BZ which contributes most to the conductance, increases quadratically with radius. Because the ring width and $T(E_t, k_{\parallel})$ within the ring remain almost constant with increasing tunnel energy E_t , the conductances increase approximately quadratically, too, as is particularly evident for $G(AP)$ [cf. the data for 0.2–1.0-eV bias in Fig. 7(b)].

However, the preceding explanation cannot explain a further interesting feature: the increase of $G(P)$ for biases of 0.6, 0.8, and 1.0 eV that occurs at tunnel energies $E_t - E_{FL}$ around 0.0, 0.2, and 0.4 eV, respectively [Fig. 7(a)]. Inspection of the transmissions and of the spectral density at $E_{FL} - 0.6$ eV produced no significant feature that would explain this behavior (this is corroborated by findings of LeClair *et al.*⁹). The feature occurs also for AP alignment [Fig. 7(b)] but not as pronounced as in the P case.

The increase with bias compensates the decrease for $E_t = E_{FL}$, as is shown for the averaged conductances G_{av} in Fig. 8(a). Whereas $G_{av}(P)$ decreases slightly (with a small minimum at zero bias), $G_{av}(AP)$ increases with $|E_b|$. Therefore the resulting TMR ρ [Eq. (12)] drops with bias, too. However, the decrease which is about 15% at 0.6 eV is

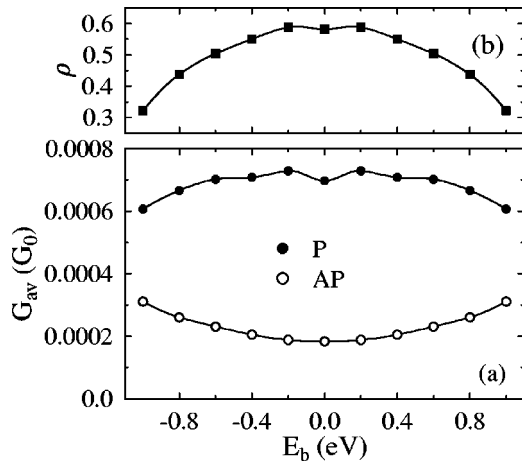


FIG. 8. Magneto-resistance of vacuum tunneling in Co(0001). (a) Averaged conductance G_{av} (in units of G_0 , the quantum of conductance) vs bias E_b for P (closed symbols) and AP (open symbols) alignment [cf. Eq. (11)]. (b) Tunnel magnetoresistance ρ vs E_b [Eq. (12)].

much less than that observed for oxide barriers. In the latter case, the TMR drops by 50 to 80% at 0.6 eV.⁴² Being due to the details of the electronic structure in the Co leads, one could term the drop in Fig. 8(b) as “DOS effect,” rather than as zero-bias anomaly.

Since inelastic processes (scattering at magnons, spin excitations) are not included in our theory, one can conclude that the ZBA found in tunnel junctions with oxide barriers can be attributed to defect scattering in the oxide barrier. This finding is consistent with the fact that the ZBA decreases with the improvement of the preparation techniques for ferromagnet-oxide interfaces (see Ref. 8 and references therein).

In a previous investigation,⁸ we used the superposition approach (Sec. II B 3) for the tunnel barrier. There, both the averaged conductances and the TMR were almost constant for biases up to 0.5 eV. Comparing with the present results that were obtained within the image-potential approach (Sec. II B 2), one has to keep in mind that details of the calculations differ (e.g., the \vec{k}_{\parallel} mesh). However, these have only minor influence. The most striking difference is the shape of the tunnel barrier which is varied in two aspects. First, the JJJ barrier used in Ref. 8 is rather smooth with respect to the interpolating Lorentzian chosen here. Generally speaking, the latter produces a larger reflection. Second, the shape in the central part of the barrier differs. In particular for large lead separations, the barrier height becomes important (cf. Figs. 3 and 5). Further, the linear bias potential which is missing in the superposition approach is expected to have a

non-negligible effect. Therefore details of the barrier are expected to have significant influence on the tunnel magnetoresistance.

IV. CONCLUDING REMARKS

We have proposed an heuristic approach for treating the bias voltage in vacuum tunneling. It keeps the first-principle description of the electrodes but replaces the cumbersome electrostatic potential of the tunnel barrier by a smooth interpolating form. The parameters of the latter can be obtained from *ab initio* calculations for the semi-infinite systems. We would like to note that the implementation of the approach in layer-KKR computer codes is straightforward, but should also be feasible in other methods (three-dimensional or screened KKR).

Recent experimental investigations by Ding and coworkers⁸ addressed the origin of the zero-bias anomaly (ZBA) which typically occurs in tunneling through oxide barriers. Using a spin-polarized scanning tunneling microscope (STM), the tunneling proceeded through the vacuum barrier between a Co(0001) surface and an amorphous STM tip. The observed absence of the ZBA provided evidence for the ZBA being mainly due to defect scattering in oxide barriers, rather than to magnon creation or spin excitations at the interfaces. The latter occur also in the STM experiment whereas defects cannot appear in the vacuum barrier. Our calculations (this work and Ref. 8) for vacuum tunneling through planar junctions showed also no ZBA, therefore corroborating the experimental results and their interpretation.

Tunnel calculations provide a rather indirect test of the proposed barrier shapes. A more direct one would be to compare theoretical energy positions and linewidths of so-called field-emission resonances⁴³ with experimental ones. These electronic states can be viewed as surface states that are trapped between the bulk (in the presence of a bulk-band gap) and the tunnel barrier between sample and an STM tip. The field-emission resonances show up as sharp maxima in the differential conductance and depend—like the shape of the tunnel barrier—on both bias voltage and tip-sample separation.

As a possible extension of the present work, one could think of a treatment of tunnel junctions with “filled” spacers (instead of vacuum), in particular with oxide barriers. Further, work is in progress to describe the tunneling with bias voltage fully on an *ab initio* level.

ACKNOWLEDGMENTS

We would like to thank Hai Feng Ding, Arthur Ernst, Ingrid Mertig, Silke Roether, Wulf Wulfhekel, and Peter Zahn for stimulating discussions.

*Corresponding author. Electronic address: henk@mpi-halle.de

¹ *Spin Dependent Transport in Magnetic Nanostructures*, edited by S. Maekawa and T. Shinjo (Taylor & Francis, London, 2002).

² J. C. Slonczewski, Phys. Rev. B **39**, 6995 (1989).

³ M. Jullière, Phys. Lett. **54A**, 225 (1975).

⁴ *Density Functional Theory*, Vol. 337 of NATO Advanced Study

Institute, Series B: Physics, edited by E. K. U. Gross and R. M. Dreizler (Plenum Press, New York, 1995).

⁵ H. R. Reiss, Phys. Rev. A **42**, 1476 (1990).

⁶ N. D. Lang, Phys. Rev. B **45**, 13 599 (1992).

⁷ W. Wulfhekel, H. F. Ding, and J. Kirschner, J. Magn. Magn. Mater. **242–245**, 47 (2002).

- ⁸H. F. Ding, W. Wulfhekel, J. Henk, P. Bruno, and J. Kirschner, *Phys. Rev. Lett.* **90**, 116603 (2003).
- ⁹P. LeClair, J. T. Kohlhepp, C. H. van de Vin, H. Wieldraaijer, H. J. M. Swagten, W. J. M. de Jonge, A. H. Davis, J. M. MacLaren, J. S. Moodera, and R. Jansen, *Phys. Rev. Lett.* **88**, 107201 (2002).
- ¹⁰O. Wunnicke, N. Papanikolaou, R. Zeller, P. H. Dederichs, V. Drchal, and J. Kudrnovský, *Phys. Rev. B* **65**, 064425 (2002).
- ¹¹K. Wang, P. M. Levy, S. Zhang, and L. Szunyogh, *Philos. Mag. B* **B83**, 1255 (2003).
- ¹²E. G. McRae and M. L. Kane, *Surf. Sci.* **108**, 435 (1981).
- ¹³E. V. Chulkov, V. M. Silkin, and P. M. Echenique, *Surf. Sci.* **437**, 330 (1999).
- ¹⁴M. Graß, J. Braun, G. Borstel, R. Schneider, H. Dürr, T. Fauster, and V. Dose, *J. Phys.: Condens. Matter* **5**, 599 (1993).
- ¹⁵L. A. Mac Coll, *Phys. Rev.* **56**, 699 (1939).
- ¹⁶We use atomic Hartree units, $e = \hbar = m = 1$, $c \approx 137.036$.
- ¹⁷P. H. Cutler and J. J. Gibbons, *Phys. Rev.* **111**, 394 (1958).
- ¹⁸R. O. Jones, P. J. Jennings, and O. Jepsen, *Phys. Rev. B* **29**, 6474 (1984).
- ¹⁹J. Rundgren and G. Malmström, *J. Phys. C* **10**, 4671 (1977).
- ²⁰G. Malmström and J. Rundgren, *Comput. Phys. Commun.* **19**, 263 (1980).
- ²¹E. Tamura and R. Feder, *Z. Phys. B: Condens. Matter* **81**, 425 (1990).
- ²²E. Tamura and R. Feder, *Vacuum* **33**, 864 (1983).
- ²³C. S. Lent and D. J. Kirkner, *J. Appl. Phys.* **67**, 6353 (1990).
- ²⁴Y. Joly, *Phys. Rev. Lett.* **68**, 950 (1992).
- ²⁵J. Henk, W. Schattke, H. Carstensen, R. Manzke, and M. Skibowski, *Phys. Rev. B* **47**, 2251 (1993).
- ²⁶S. Lorenz, C. Solterbeck, W. Schattke, J. Burmeister, and W. Hackbusch, *Phys. Rev. B* **55**, R13 432 (1997).
- ²⁷*Handbook of Mathematical Functions*, edited by M. Abramowitz and I. A. Stegun (Dover Publications, New York, 1970).
- ²⁸L. Limot, T. Maroutian, P. Johansson, and R. Berndt, *Phys. Rev. Lett.* **91**, 196801 (2003).
- ²⁹J. M. MacLaren, X.-G. Zhang, W. H. Butler, and X. Wang, *Phys. Rev. B* **59**, 5470 (1999).
- ³⁰M. Büttiker, *Phys. Rev. Lett.* **57**, 1761 (1986).
- ³¹J. Henk, in *Handbook of Thin Film Materials*, edited by H. S. Nalwa (Academic Press, San Diego, 2001), Vol. 2, Chap. 10, p. 479.
- ³²J. Henk, *Phys. Rev. B* **64**, 035412 (2001).
- ³³C. Math, J. Braun, and M. Donath, *Surf. Sci.* **482–485**, 556 (2001).
- ³⁴J. Braun and M. Donath, *Europhys. Lett.* **59**, 592 (2002).
- ³⁵S. N. Okuno, T. Kishi, and K. Tanaka, *Phys. Rev. Lett.* **88**, 066803 (2002).
- ³⁶S. G. Davison and M. Stęślička, *Basic Theory of Surface States* (Clarendon, Oxford, 1992).
- ³⁷D. W. Jepsen and P. M. Marcus, in *Computational Methods in Band Theory*, edited by P. M. Marcus, J. F. Janak, and A. R. Williams (Plenum Press, New York, 1971), p. 416.
- ³⁸P. Weinberger, *Electron Scattering Theory of Ordered and Disordered Matter* (Clarendon Press, Oxford, 1990).
- ³⁹J. C. Slater, *Phys. Rev.* **51**, 840 (1937).
- ⁴⁰V. Heine, *Proc. Phys. Soc. London* **81**, 300 (1963).
- ⁴¹A. H. Davis and J. M. MacLaren, *J. Appl. Phys.* **87**, 5224 (2000).
- ⁴²S. Yuasa, T. Nagahama, and Y. Suzuki, *Science* **297**, 234 (2002).
- ⁴³J. W. Gadzuk, *Phys. Rev. B* **47**, 12 832 (1993).